PCCP

Flow-distributed oscillation patterns in the Oregonator model

J. R. Bamforth,[a] J. H. Merkin,[a] S. K. Scott,*[a] R. Tóth[b] and V. Gáspár[b]

[a] *School of Chemistry and Department of Applied Mathematics, University of Leeds, Leeds, UK LS2 9JT*
[b] *Institute of Physical Chemistry, University of Debrecen, 4010 Debrecen, P.O. Box 7, Hungary*

Received 18th December 2000, Accepted 28th February 2001
First published as an Advance Article on the web 20th March 2001

The conditions under which chemical patterns corresponding to "flow-distributed oscillations" are formed are determined analytically for the Oregonator model of the Belousov–Zhabotinsky reaction. These analytical results are confirmed by numerical computation and are also used to predict typical values for the critical flow velocity and how the wavelength varies with the concentrations of the major reactants.

1. Introduction

The concept of chemical pattern formation through "flow-distributed oscillations" (FDO) was proposed recently by Kuznetsov *et al.*[1] and demonstrated through an analysis of the Brusselator model by Andresen *et al.*[2] Subsequently, Kaern and Menzinger[3] have realised such patterns experimentally using the Belousov–Zhabotinsky (BZ) reaction and shown general agreement between experiment and a limited set of numerical computations based on the Zhabotinsky–Rovinsky[4] model for this reaction. Satnoianu and Menzinger[5] have extended this idea to include differential diffusion—based on an electric field model[6]—relating the FDO mechanism to Turing patterns, and introduced a class of patterns they call "flow induced structures". Bamforth *et al.*[7] have shown that FDO structures can be predicted for the chlorine dioxide–iodine–malonic acid (CDIMA) reaction for realistic experimental conditions. In their paper, these authors also derived general formulae for the critical conditions for the onset of stationary patterns and also for other spatiotemporal responses in this experimental configuration.

In this short paper, we apply the formulae derived by Bamforth *et al.* to the Oregonator model[7] for the BZ system. In addition to its role with regard to the BZ system, the Oregonator has developed the status of a paradigm model for excitable media in general.

2. Governing equations and stability analysis

The appropriate form of the governing equations for the Oregonator model[8] in a system with reaction, diffusion and advection in the Tyson–Fife[9] scalings is as follows:

$$\frac{\partial u}{\partial t} = \frac{\partial^2 u}{\partial x^2} - \phi_P \frac{\partial u}{\partial x} + \frac{1}{\varepsilon}\left\{u(1-u) - fv\frac{(u-q)}{(u+q)}\right\} \quad (1a)$$

$$\frac{\partial v}{\partial t} = \frac{\partial^2 v}{\partial x^2} - \phi_P \frac{\partial v}{\partial x} + u - v \quad (1b)$$

(see also ref. 10). Here u and v represent the dimensionless concentrations of the autocatalyst ($HBrO_2$) and the oxidised form of the catalyst (M_{ox}) respectively and the parameters ε, f and q have their normal meanings in terms of the concentrations of the major reactant species and reaction rate coefficients for this model. For simplicity, we assume equal diffusion coefficients and flow velocity (ϕ_P in dimensionless form) for each species. Time and distance are made dimensionless with respect to the time and space scales: $t_{ref} = (k_c B)^{-1}$ and $x_{ref} = (D/k_c B)^{1/2}$ respectively, where k_c is the rate coefficient for "process c" and B represents the total concentration of organic species, D is the molecular diffusion coefficient. The parameter ε is given by $k_c B/k_5 A$ where k_5 is the rate coefficient for the autocatalytic step in "process b" and A is the concentration of bromate ion. Typical values are $k_c = 1$ M^{-1} s^{-1} and $k_5 = 8$ M^{-1} s^{-1} corresponding to a system in which $[H^+] = 0.8$ M and, from Kaern and Menzinger,[3] we adopt $A = 0.2$ M and $B = 0.4$ M, giving $\varepsilon = 0.25$.

The uniform steady state of eqn. 1(a,b) satisfies

$$u_{ss} = v_{ss} = \tfrac{1}{2}\{1 - f - q + [(1-f-q)^2 + 4q(1+f)]^{1/2}\} \quad (2)$$

Following the analysis in Bamforth *et al.*,[7] we obtain the linearised equations governing the evolution of small perturbations about this steady state in the form

$$\frac{\partial U}{\partial t} = \frac{\partial^2 U}{\partial x^2} - \phi_P \frac{\partial U}{\partial x} + \frac{1}{\varepsilon}\{\alpha U - \beta V\} \quad (3a)$$

$$\frac{\partial V}{\partial t} = \frac{\partial^2 V}{\partial x^2} - \phi_P \frac{\partial V}{\partial x} + U - V \quad (3b)$$

where $u = u_{ss} + U$ and $v = v_{ss} + V$. The coefficients α and β are given by

$$\alpha = 1 - 2u_{ss} - 2f\frac{u_{ss}q}{(u_{ss}+q)^2}, \quad \beta = f\frac{(u_{ss}-q)}{(u_{ss}+q)} \quad (4)$$

where α and β depend only on f and q. We may then define the Jacobian matrix $\boldsymbol{J}$ in the form

$$\boldsymbol{J} = \begin{pmatrix} \alpha/\varepsilon & -\beta/\varepsilon \\ 1 & -1 \end{pmatrix} \quad (5)$$

with $\mathrm{Tr} = (\alpha/\varepsilon) - 1$ and $\Delta = (\beta - \alpha)/\varepsilon$ being the trace and determinant. The system will be "kinetically stable", *i.e.* there will be a stable steady state in a well-stirred batch configuration, if $\mathrm{Tr} < 0$ and $\Delta > 0$.

3. Stability condition

Following the analysis in ref. 7, the critical flow velocity $\phi_P = \phi_{AC}$ for the transition from absolute to convective instability is

given by

$$\phi_{AC} = \sqrt{2\ \mathrm{Tr}} = \sqrt{2(\alpha - \varepsilon)/\varepsilon} \tag{6}$$

Similarly, the condition for the bifurcation to stationary patterns $\phi_P = \phi_{P,\,cr}$ is given by

$$\phi_{P,\,cr} = \sqrt{\frac{4\Delta - \mathrm{Tr}^2}{2\ \mathrm{Tr}}} = \sqrt{\frac{4\varepsilon\beta - (\alpha + \varepsilon)^2}{2(\alpha - \varepsilon)\varepsilon}} \tag{7}$$

Both conditions (6) and (7) require $\alpha > \varepsilon$ and we may note that the condition $\alpha = \varepsilon$ is the Hopf bifurcation condition for the corresponding well-stirred batch system.

The loci corresponding to conditions (6) and (7) in the ϕ_P–ε parameter plane are shown in Fig. 1 for a system with $f = 1$ and $q = 0.0008$. The corresponding batch system has $\alpha = 0.888$, and the locus for the bifurcation to stationary patterns shows a vertical asymptote at $\varepsilon = \alpha$. For $\varepsilon < \alpha$, the two loci divide the parameter plane into four regions. Stationary patterns are found in the region above both loci. In the region below both loci, the system is absolutely unstable. In the small region to the right of the diagram, above the locus corresponding to eqn. (6) but below that for eqn. (7), the system is convectively unstable. Finally, in the region at low ε and ϕ_P, above the locus corresponding to eqn. (7) but below that for eqn. (6) the system shows "transient waves" (see later). We may also note that the critical flow velocity given by eqn. (7) passes through zero for $\varepsilon = 0.490$ when $\varepsilon = 2\beta - \alpha - [4\beta(\beta - \alpha)]^{1/2}$, and also that the two loci cross at $\varepsilon = 0.676$ when $5\varepsilon^2 - 2(3\alpha + 2\beta)\varepsilon + 5\alpha^2 = 0$.

Example space–time plots for parameter values from various points on Fig. 1 are shown in Fig. 2 and 3. The distinction between absolutely unstable, convectively unstable and stationary patterns is most easily demonstrated by taking a relatively large value of ε, above the value at which the two loci cross, so we take $\varepsilon = 0.8$. With $\phi_P = 0.2$, the system is absolutely unstable and a perturbation applied at the origin of the plug flow section of the reactor propagates along the tube leaving a response approaching a spatially-uniform oscillation in time that persists for all subsequent time, Fig. 2(a). In this grey scale plot, the lighter regions correspond to high concentration of the oxidised form of the redox catalyst and the dark indicates a reduced state. For $\phi_P = 0.8$, the system is convectively unstable, so the perturbation disturbs the system from its initial uniform state, but at each point the system eventually returns to its original state, Fig. 2(b)—this return is evident for $t > 120$ starting at $x \approx 55$.

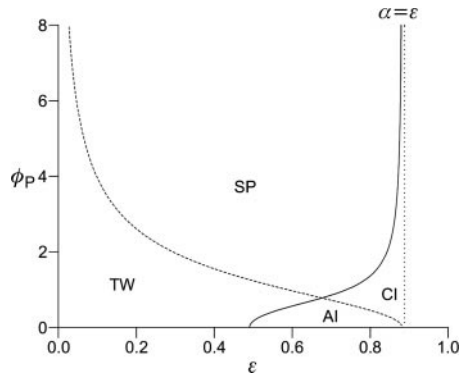

Fig. 1 The bifurcation loci for the transition from absolute instability (AI) to convective instability (CI) and for the transition to stationary patterns (SP) in the ϕ_P–ε parameter plane: dashed curve, ϕ_{AC} as given by eqn. (6); solid curve, $\phi_{P,\,cr}$ as given by eqn. (7). The region labelled TW corresponds to transient waves.

There is, however, a boundary layer over $0 < x < 50$ in which a stationary pattern is established by the steady state conditions at the inflow. At longer times, the "horizontal" black and white stripes will move completely out of the domain and a steady state is observed for $x > 50$.

(The perturbation at the origin comprises the imposition of a boundary condition corresponding to the steady state solution for this reaction model in the continuously-fed stirred tank reactor (CSTR) which feeds the plug-flow reactor. In all the computations described here, we take a dimensionless residence time $\phi_c = 1.0$ to provide the steady state condition. Further details of this approach have been given in the paper by Bamforth *et al.*[7] We may note that the long-time responses observed are essentially independent of the perturbation imposed.)

With $\phi_P = 3.0$ the flow rate exceeds the critical value given by eqn. (7) and a stationary pattern develops, as shown in Fig. 2(c). The wavelength adopted is equal to the product of the flow rate and the oscillatory period t_p observed in the corresponding batch system ($t_P = 19.2$), as expected from previous analysis.[3,7] The change in wavelength with the oscillatory period can be seen by comparing Fig. 2(c) with Fig. 3(a), corresponding to $\varepsilon = 0.25$, a value typical of the experiments reported by Kaern and Menzinger[3] and for which $t_p = 9.0$. Finally, with $\varepsilon = 0.25$ but at a lower flow rate, $\phi_P = 0.8 < \phi_{AC}$, a transient wave pattern emerges, Fig. 3(b), which initially has the appearance of phase waves propagating down the tube (increasing x in time) but develops into waves with negative gradient on the diagram. This is a somewhat surprising observation as it implies waves travelling "against" the imposed fluid flow, but is a true asymptotic feature of this model (it was not observed in the previous computations for the CDIMA model[7]). The wavelength of the TW patterns is much longer than would be predicted simply on the basis of the oscillatory frequency and the flow velocity.

The parameter ε can be varied between experiments through variation of the ratio of initial concentrations of the

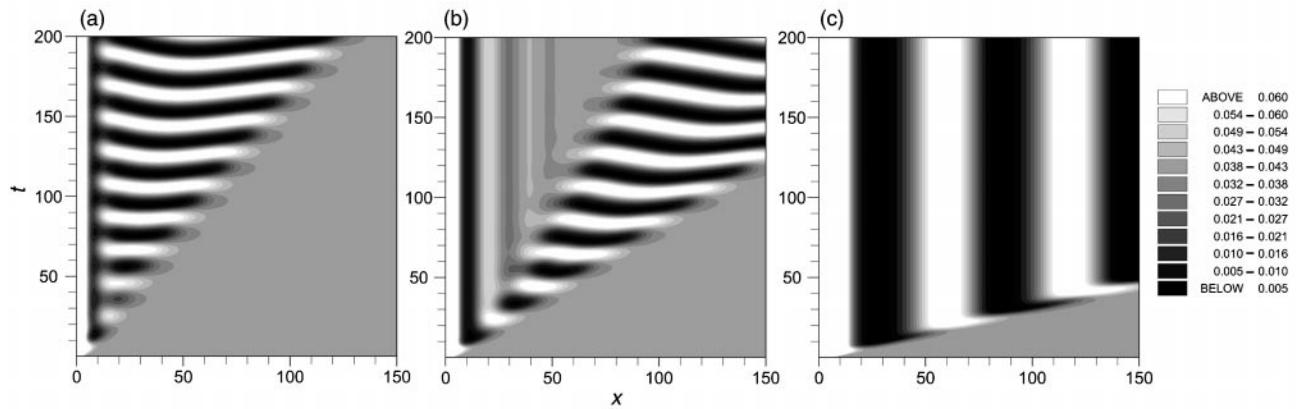

Fig. 2 Space–time plots for a system with $f = 1$ and $\varepsilon = 0.8$. (a) $\phi_P = 0.2$, corresponding to region of absolute instability; (b) $\phi_P = 0.8$, corresponding to region of convective instability; (c) $\phi_P = 3.0$, corresponding to region of stationary patterns. The dark regions correspond to the reduced state of the redox catalyst and light to the oxidised state.

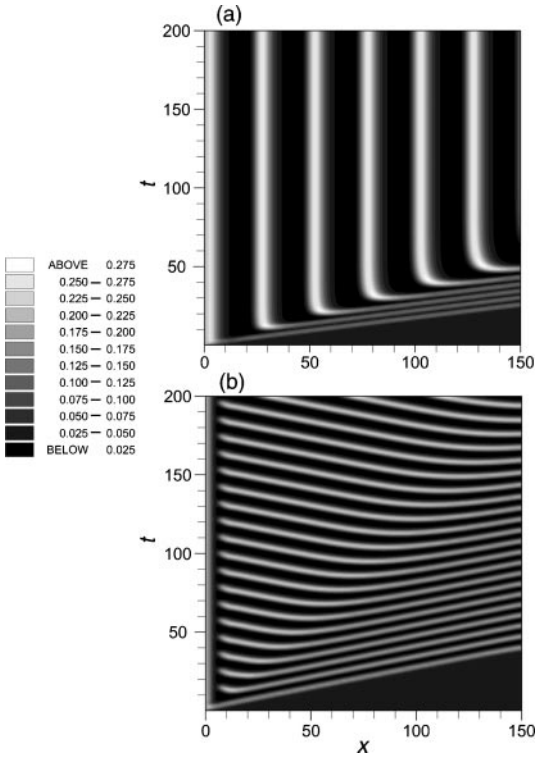

Fig. 3 Space–time plots for a system with $f = 1$ and $\varepsilon = 0.25$. (a) $\phi_P = 3.0$, the wavelength here can be compared with that in Fig. 2(c) for the same flow rate; (b) $\phi_P = 0.8$, corresponding to region of transient waves. Note that the grey scale corresponds to a different range of concentrations for the redox catalyst from that in Fig. 2, but again dark regions correspond to the reduced state of the redox catalyst and light to the oxidised state.

organic reducing species to those of bromate and H^+ ions. The so-called "stoichiometric parameter" f which indicates the number of bromide ions produced per two oxidised metal ions reduced can also be varied experimentally by changing the initial concentration of bromomalonic acid in the system. Fig. 4(a,b) shows the bifurcation loci corresponding to conditions (6) and (7) in the ϕ_P–f parameter plane for two different

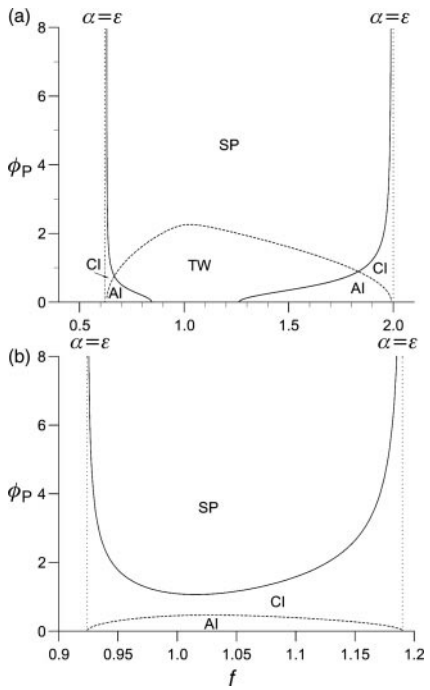

Fig. 4 The bifurcation loci in the ϕ_P–f parameter plane: (a) $\varepsilon = 0.25$, (b) $\varepsilon = 0.8$.

values of ε, namely $\varepsilon = 0.25$ typical of the experiments of Kaern and Menzinger, and $\varepsilon = 0.8$ respectively.

With $\varepsilon = 0.25$, there are Hopf bifurcation points for the equivalent batch reactor system when $\alpha = \varepsilon$ corresponding to $f = 0.630$ and $f = 1.990$. Flow distributed structures are possible only for values of f within this range under the present conditions (equal diffusivities). Eqn. (7) indicates positive minimum flow velocities for $0.630 < f < 0.844$ and for $1.262 < f < 1.990$. These loci are crossed by that for condition (6) once on each branch. The parameter plane is thus divided into six regions—one for stationary patterns, two each for convective and absolute instability (one of each at high f and one of each at low f) with the system passing from absolute through convective and then to stationary patterns as ϕ_P is increased at constant f, and one region of transient waves bounded by the crossing points of the two sets of loci.

With $\varepsilon = 0.8$, Hopf bifurcations in the equivalent batch reactor occur at $f = 0.924$ and 1.190, so the various types of FDO structure are found only within these limits. The loci governed by eqn. (6) and (7) do not cross in this case, with $\phi_{P,cr} > \phi_{AC}$ for all f across the above range. There are thus only three regions: the region of absolute instability for $\phi < \phi_{AC}$, the region of convective instability for $\phi_{AC} < \phi_P < \phi_{P,cr}$ and the region of stable, stationary patterns for $\phi_P > \phi_{P,cr}$.

4. Discussion and conclusions

The computations above indicate that the conditions for a variety of spatiotemporal responses can be determined analytically for the Oregonator model of the BZ reaction. The methodology followed here could be applied to any two-variable model possessing a batch Hopf bifurcation. Fig. 1 and 4 indicate how the parameter plane can be divided into different regions for each type of response. Of particular interest are the "stationary patterns" representing the "flow-distributed oscillations". Previous theory has indicated the existence of a minimum or critical flow rate for such patterns to be stabilised. Below this critical flow rate, transient waves are observed. These are not, however, the same type of transient wave reported by Kaern and Menzinger, who observed waves which were caused by an oscillatory instability arising in the CSTR thus giving a time-dependent inflow or boundary condition for the plug-flow reactor.

The simple relationship between the flow rate, the natural oscillatory period and the wavelength seen in our previous work on the CDIMA reaction emerges again in the above computations. This has the benefit that the wavelength of the flow-distributed oscillation pattern can be predicted simply by determining the oscillatory period from the ordinary differential equations for the well-stirred batch system rather than requiring solution of the partial-differential plug-flow equations. The simplicity of the Oregonator model allows us to predict the variation of the oscillatory period on the parameters ε and f analytically for systems close to the Hopf bifurcation points for which the natural oscillatory period is given by $2\pi/\Delta^{1/2}$ with $\Delta = (\beta - \varepsilon)/\varepsilon$ from the definition of Δ given previously and the Hopf condition $\alpha = \varepsilon$. Developing the analysis given by Leach *et al.*,[11] for systems with $f < 1$, $u_s \gg q$ and so $\beta \approx f = (1 + \varepsilon)/2$ at the Hopf point, giving $t_p \sim 2\pi\sqrt{2\varepsilon/(1 - \varepsilon)}$ which provides an excellent estimate (within 5%) of the computed oscillatory period for all $f < 1$ and $\varepsilon < 0.85$ for a system with $q \ll 1$.

Since parameter ε is defined as $k_c B/k_5 A$,

$$\bar{t}_p = \frac{t_p}{k_c B} \sim \frac{\sqrt{\varepsilon/(1-\varepsilon)}}{k_c B} = \frac{\sqrt{k_c B/k_5 A}}{k_c B\sqrt{(1 - k_c B/k_5 A)}}$$

$$= \sqrt{\frac{1}{k_c B(k_5 A - k_c B)}}.$$

the period $\bar{t}_p$ should then scale as $[k_c B(k_5 A - k_c B)]^{-1/2}$, and the FDO wavelength would then scale as $f_p[k_c B(k_5 A - k_c B)]^{-1/2}$, where f_p is the dimensional flow rate.

Experiments are more commonly performed for compositions corresponding to conditions close to the reduced steady state, *i.e.* with $f > 1$. Under these conditions, again developing the analysis from Leach *et al.*,[11] we have $\beta \approx 1$ and so the natural period is expected to scale as $t_p \sim 2\pi\sqrt{\varepsilon/(1-\varepsilon)}$. Again, this gives an excellent estimate of the actual period for systems with $f > 1$ and $\varepsilon < 0.85$ for $q \ll 1$ and again the dimensional period and wavelength are expected to scale as $[k_c B(k_5 A - k_c B)]^{-1/2}$ and $f_p[k_c B(k_5 A - k_c B)]^{-1/2}$ respectively along the Hopf curve for constant flow rate. Somewhat more crudely, if $k_5 A \gg k_c B$ (which is not always satisfied in the experiments of Kaern and Menzinger), the period and wavelength should scale approximately as $1/\{[BrO_3^-][H^+][Org]\}^{1/2}$.

The above relationships apply only if ε and f are simultaneously varied in an experiment so as to stay close to the Hopf bifurcation locus. To investigate the variation of the oscillatory period with ε and f generally within the region of oscillatory batch behaviour, the governing rate equations for the Oregonator model have to be integrated numerically. Fig. 5 indicates the Hopf bifurcation loci for a system with $q = 0.0008$ enclosing the region of spontaneous oscillatory behaviour in a batch system and hence the parameter range for which FDO patterns can be observed. The variation of the dimensionless period t_p across this region is indicated. For constant f, the period increases monotonically with increasing ε. Experimentally this may be achieved by decreasing $[H^+]$ or $[BrO_3^-]$. The data in selected regions of Fig. 5 can be fitted by a log–log plot which indicates that the dimensionless period scales approximately as $\varepsilon^{1/2}$, which would imply that the dimensional period and wavelength scale as $\{[BrO_3^-][H^+]\}^{-1/2}$ and would be independent of [Org]. For experiments at constant ε with varying f, corresponding approximately to varying the ratio of malonic to bromomalonic acid at constant $[H^+]$, $[BrO_3^-]$ and total organic species concentration, the dimensionless period is approximately constant over much of the range except near the Hopf bifurcation points.

The choice of k_c and the applicability of the Oregonator model for the ferroin system has been discussed elsewhere.[12,13] Taylor *et al.*[14] have estimated an appropriate rate coefficient on the basis of the decay of the spatial profile in the rear of the chemical wave pulse for this system (see also Ungvárai *et al.*[15]) giving $k_c = 2.64\ M^{-1}\ s^{-1}$. This yields an oscillatory period of 60.1 s, based on $B = 0.4$ M, $\varepsilon = 0.25$ and the estimate $f = 1$. This compares as well as can be expected with the experimentally measured period of 130 s. The scaling with the reactant concentrations derived here can be expected

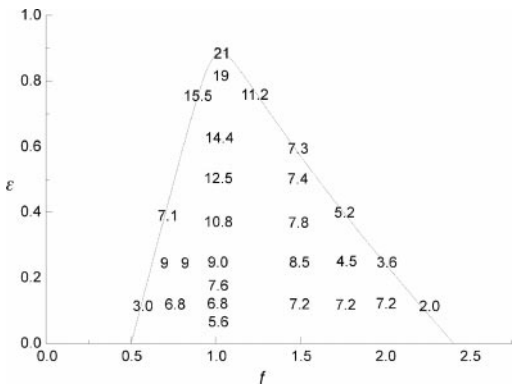

Fig. 5 The Hopf bifurcation locus in the f–ε parameter plane for the well-stirred batch system with $q = 0.0008$. The numbers indicate the dimensionless oscillatory period computed numerically or from the Hopf bifurcation condition.

to predict the FDO wavelengths to similar precision and the functional dependences on the concentrations should certainly be testable experimentally. Taylor *et al.*[14] also note that the consumption of the reduced form of the redox catalyst is important in the ferroin-catalysed system (it is neglected in the simple Oregonator form). Andresen *et al.*[16] have performed computations of FDO patterns using the Rovinsky–Zhabotinsky[4] model. They found a nonlinear relationship between the FDO wavelength and the flow velocity at least for conditions close to critical flow rate. This is an interesting difference between the two models. The RZ model is generally a more suitable model for the ferroin-catalysed BZ system and so an investigation of this aspect experimentally would be of great interest.

The critical flow rate rises to relatively high values in the vicinity of the Hopf bifurcation condition ($\alpha = \varepsilon$ for the present model), but decreases away from such points. To a reasonable level of approximation, we may conclude that a typical value for the critical flow rate for Oregonator-based systems is $\phi_{P,cr} \approx 2$. This can be converted to a dimensional value f_p using the scalings described earlier, $f_p = (Dk_c B)^{1/2}\phi_P \approx (0.005\ cm\ s^{-1})\phi_P$ taking $k_c = 2.64\ M\ s^{-1}$, $B = 0.4$ M and $D = 2 \times 10^{-5}\ cm^2\ s^{-1}$. Thus an estimate of the critical flow velocity is $f_{p,cr} = 0.01\ cm\ s^{-1}$.

Taking the experimental configuration of Kaern and Menzinger,[3] comprising a tube of 10 mm inner diameter and assuming 33% free volume (the volume of the tube not occupied by the beads used to ensure plug flow), such that the free volume per unit length of the tube is 0.26 mL cm^{-1}, then this translates to a critical volumetric flow rate of *ca.* 0.14 mL min^{-1}.

Such flows are difficult to maintain in practice, suggesting that the existence of a minimum flow would be difficult to demonstrate experimentally except for systems close to the batch Hopf condition: Kaern and Menzinger do not report any experimental observation of the critical flow rate.

Acknowledgements

This work was supported by the British Council and the Hungarian Scholarship Board (Ministry of Education) under the Joint Academic Research Programme (project no. 010), by the ESF Scientific Programme REACTOR and by the Hungarian Research Grants OTKA T025375 and FKFP 0455/1997.

References

1 S. P. Kuznetsov, E. Mosekilde, G. Dewel and P. Borckmans, *J. Chem. Phys.*, 1997, **106**, 7609.
2 P. Andresen, M. Bache, E. Mosekilde, G. Dewel and P. Borckmans, *Phys. Rev. E*, 1999, **60**, 297.
3 M. Kaern and M. Menzinger, *Phys. Rev. E*, 1999, **60**, R3471.
4 A. M. Zhabotinsky and A. B. Rovinsky, *J. Phys. Chem.*, 1990, **94**, 8001.
5 R. A. Satnoianu and M. Menzinger, *Phys. Rev. E*, 2000, **62**, 113.
6 J. H. Merkin, R. A. Satnoianu and S. K. Scott, *Dyn. Stab. Syst.*, 2000, **15**, 209.
7 J. R. Bamforth, S. Kalliadasis, J. H. Merkin and S. K. Scott, *Phys. Chem. Chem. Phys.*, 2000, **2**, 4013.
8 R. J. Field and R. M. Noyes, *J. Chem. Phys.*, 1974, **60**, 1877.
9 J. J. Tyson and P. C. Fife, *J. Chem. Phys.*, 1980, **73**, 2224.
10 R. Tóth, A. Papp, V. Gáspár, J. H. Merkin, S. K. Scott and A. F. Taylor, *Phys. Chem. Chem. Phys.*, 2001, **3**, 957.
11 J. A. Leach, J. H. Merkin and S. K. Scott, *Philos. Trans. R. Soc. London, Ser. A*, 1993, **345**, 229.
12 N. Ganapathisubramanian and R. M. Noyes, *J. Phys. Chem.*, 1982, **86**, 5158.
13 Y.-C. Chou, H.-P. Lin, S. S. Sun and J.-J. Jwo, *J. Phys. Chem.*, 1993, **97**, 8450.
14 A. F. Taylor, V. Gáspár, B. R. Johnson and S. K. Scott, *Phys. Chem. Chem. Phys.*, 1999, **1**, 4595.
15 J. Ungvárai, Zs. Nagy-Ungvárai, J. Enderlein and S. C. Müller, *J. Chem. Soc., Faraday Trans.*, 1997, **93**, 69.
16 P. Andresen, E. Modekilde, G. Dewel and P. Borckmans, *Phys. Rev. E*, 2000, **62**, 2992.